# High-Performance Solar-Blind Photodetectors Based on $Al_xGa_{1-x}N$ Heterostructures

Ekmel Ozbay, *Member, IEEE*, Necmi Biyikli, *Student Member, IEEE*, Ibrahim Kimukin, *Student Member, IEEE*, Tolga Kartaloglu, *Member, IEEE*, Turgut Tut, and Orhan Aytür, *Member, IEEE*

*Invited Paper*

***Abstract*—Design, fabrication, and characterization of high-performance $Al_xGa_{1-x}N$-based photodetectors for solar-blind applications are reported. $Al_xGa_{1-x}N$ heterostructures were designed for Schottky, p-i-n, and metal–semiconductor–metal (MSM) photodiodes. The solar-blind photodiode samples were fabricated using a microwave compatible fabrication process. The resulting devices exhibited extremely low dark currents. Below 3 fA, leakage currents at 6-V reverse bias were measured on p-i-n samples. The excellent current–voltage ($I$–$V$) characteristics led to a detectivity performance of $4.9\times10^{14}$ cmHz$^{1/2}$W$^{-1}$. The MSM devices exhibited photoconductive gain, while Schottky and p-i-n samples displayed 0.09 and 0.11 A/W peak responsivity values at 267 and 261 nm, respectively. A visible rejection of $2\times10^4$ was achieved with Schottky samples. High-speed measurements at 267 nm resulted in fast pulse responses with greater than gigahertz bandwidths. The fastest devices were MSM photodiodes with a maximum 3-dB bandwidth of 5.4 GHz.**

***Index Terms*—AlGaN, detectivity, heterostructure, high speed, metal–semiconductor–metal (MSM), photodetector, p-i-n, Schottky, solar blind, ultraviolet.**

## I. Introduction

THE SUN is a strong source of ultraviolet (UV) radiation. Thanks to the ozone layer, we are not exposed to the harmful portion of the solar UV radiation. The ozone layer acts as a natural low-pass filter by absorbing the high-energy solar photons with wavelengths smaller than ~280 nm [1]. Photodetectors which respond only to radiation with $\lambda < 280$ nm are defined as solar-blind photodetectors. Within the atmosphere, such a detector would not detect any solar radiation. Hence, if a solar-blind photodetector detects a signal, this is a sign of an external UV emitter flame, missile plume, etc. [2].

The immunity from solar interference makes solar-blind detectors unique for a wide range of commercial and military applications: environmental (ozone layer) monitoring, flame detection/fire alarms, sterilization/detection of biological and chemical agents, engine monitoring, missile plume detection, secure intersatellite communications, and underwater/submarine communication systems [3]. These applications require high-performance solar-blind photodetectors with low dark current, high responsivity, high detectivity, and high bandwidth.

Solar-blind detection was traditionally accomplished by photomultiplier tubes (PMTs) and silicon photodiodes. With the advent in material growth of high-quality $Al_xGa_{1-x}N$ ternary alloys [4]–[14], AlGaN-based wide bandgap solar-blind photodetectors emerged as a potential alternative for the PMT and Si-based detector technology. The long wavelength cutoff of $Al_xGa_{1-x}N$ can be tuned from 360 to 200 nm by increasing the Al content and for $x > 0.38$, AlGaN becomes intrinsically solar blind. Therefore, unlike PMT and Si technology, AlGaN-based solar-blind detectors do not need complex and costly filters. In addition, they can operate under harsh conditions (high temperature and power levels) due to their wide bandgap and robust material properties [15]. These features made the $Al_xGa_{1-x}N$ material system the choice for the realization of high-performance solar-blind detectors.

The first AlGaN-based solar-blind photodetectors were demonstrated in 1996 [16], [17]. Both detectors were AlGaN-based photoconductors with true solar-blind characteristics. Thereafter, several research groups have contributed to the performance of solar-blind AlGaN photodetectors. Schottky [18]–[23], p-i-n [24]–[38], MSM [39]–[44], and p-n junction [45] types of photodiodes with excellent detection characteristics were reported. Very low dark currents at the femtoampere level [22], [35], [36], [39] and high solar-blind responsivity performance [29], [33], [37] resulted in extremely high detectivity values which could not be achieved with conventional narrow bandgap semiconductor-based detectors. High visible rejection of more than six orders of magnitude [25], [45] and low cutoff wavelengths down to 225 nm [25] were also successfully reported. Noise performance of high-quality solar-blind AlGaN detectors are far beyond the limit of the state of the art measurement setups. In terms of high-speed performance, AlGaN solar-blind detectors with a gigahertz-level frequency response have been reported recently [22], [23].

In this paper, we present our research efforts on high-performance AlGaN-based solar-blind photodiodes. Schottky, p-i-n, and MSM structures were designed, fabricated, and characterized. Solar-blind detectors with record low dark current density, solar-blind detectivity, and 3-dB bandwidth performance are demonstrated.

Manuscript received January 23, 2004; revised May 11, 2004.

This work was supported in part by NATO under Grant SfP971970, by the Turkish Department of Defense under Grant KOBRA-002, and by FUSAM-03. The work of E. Ozbay was supported by the Turkish Academy of Sciences.

E. Ozbay, I. Kimukin, and T. Tut are with the Department of Physics, Bilkent University, Bilkent, Ankara 06800, Turkey.

N. Biyikli, T. Kartaloglu, and O. Aytür are with the Department of Electrical and Electronics Engineering, Bilkent University, Bilkent, Ankara 06800, Turkey (e-mail: biyikli@ee.bilkent.edu.tr).

Digital Object Identifier 10.1109/JSTQE.2004.831681

TABLE I
ALGAN SCHOTTKY PHOTODIODE STRUCTURE

| Material | Thickness | Doping ($cm^{-3}$) |
|---|---|---|
| $Al_{0.38}Ga_{0.62}N$ | 0.8 μm | N– ($1\times10^{16}$ $cm^{-3}$) |
| $Al_{0.38}Ga_{0.62}N$ | 0.2 μm | N+ ($2\times10^{18}$ $cm^{-3}$) |
| GaN | 0.6 μm | N+ ($2\times10^{18}$ $cm^{-3}$) |
| GaN | 0.5 μm | u. i. d. |
| AlN nucleation layer | <100 nm | u. i. d. |
| Sapphire substrate | ~300 μm | – |

TABLE II
ALGAN P-I-N PHOTODIODE STRUCTURE

| Material | Thickness | Doping ($cm^{-3}$) |
|---|---|---|
| GaN | 30 nm | P+ (>$1\times10^{17}$ $cm^{-3}$) |
| $Al_{0.45}Ga_{0.55}N \rightarrow GaN$ | 15 nm | P+ (>$1\times10^{17}$ $cm^{-3}$) |
| $Al_{0.45}Ga_{0.55}N$ | 10 nm | P+ (>$1\times10^{17}$ $cm^{-3}$) |
| $Al_{0.45}Ga_{0.55}N$ | 100 nm | u. i. d. |
| GaN | 250 nm | N+ ($2\times10^{18}$ $cm^{-3}$) |
| AlN nucleation layer | 100 nm | u. i. d. |
| Sapphire substrate | ~300 μm | – |

## II. EXPERIMENTAL WORK

### A. Design

The epitaxial structures of AlGaN photodiodes were designed to achieve true solar blindness with cutoff wavelengths smaller than 280 nm. To fulfill this requirement, $Al_xGa_{1-x}N$ absorption layers with $x > 0.38$ were utilized. Table I shows the layer structure of AlGaN Schottky photodiode. The active layer is a 0.8-$\mu$m-thick $Al_{0.38}Ga_{0.62}N$ layer. A highly doped GaN layer was used for ohmic contact region due to the difficulty of obtaining high-quality ohmic contacts with $Al_xGa_{1-x}N$ layers. The n-type doped 0.2-$\mu$m-thick $Al_{0.38}Ga_{0.62}N$ layer acted as a diffusion barrier for the photo carriers generated in the GaN ohmic contact layer. This diffusion barrier was inserted to increase the visible rejection of the detector.

The AlGaN p-i-n photodiode was also designed for front illumination. The epitaxial structure of the p-i-n detector is shown in Table II. The main disadvantage of AlGaN-based p-i-n detectors is the difficulty of forming high-quality ohmic contacts to p-type doped AlGaN layers. To minimize this difficulty, a thin p+ GaN cap layer was added on top of p+ AlGaN layer. This cap layer reduces the quantum efficiency performance by absorption and makes the detector slower by the diffusion of photogenerated carriers. However, these drawbacks can be eliminated by the recess etch of the cap layer after device fabrication. To minimize carrier trapping at the p+ GaN–AlGaN interface, a thin graded layer was designed. The absorption layer used in p-i-n structure was formed by a 100-nm-thick unintentionally doped $Al_{0.45}Ga_{0.55}N$ layer. For n+ ohmic contacts, similar to Schottky design, an n-type doped GaN layer was used.

The AlGaN MSM photodiode structure was simpler than Schottky and p-i-n designs. The detector active layer was designed to be a 1.0-$\mu$m-thick unintentionally doped $Al_{0.38}Ga_{0.62}N$ layer which was grown on top of a ~2.0 $\mu$m thick GaN buffer layer. The thick buffer layer was grown to reduce the defect density in the subsequent AlGaN layer.

The $Al_xGa_{1-x}N$/GaN epitaxial layers of the heterojunction photodiode wafers were grown on a 2-in single-side polished (0001) sapphire substrate using metal–organic chemical vapor deposition (MOCVD).

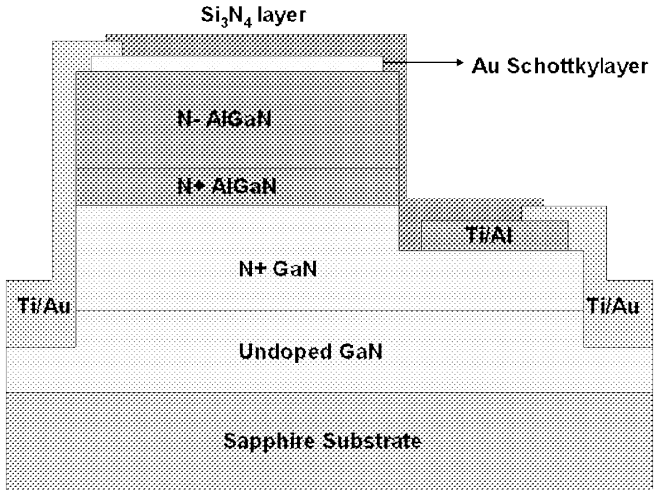


Fig. 1. Cross-sectional schematic of the completed AlGaN solar-blind Schottky photodiode.

### B. Fabrication Process

A five-level microwave compatible fabrication process was used for Schottky and p-i-n photodiode samples [22], [46], [36]. MSM detector samples were fabricated by using four mask levels. For Schottky and p-i-n samples, the fabrication started with the formation of n+ ohmic contacts. First, the ohmic patterns were defined and etched down to the n+ GaN layer. Dry etching with $CCl_2F_2$ gas was utilized in a reactive ion etching (RIE) system. The Ti–Al alloy was evaporated and after liftoff process, thermal annealing at 700 °C was applied for 30 s in a rapid thermal annealing (RTA) system. The second step was the Schottky contact and p+ ohmic contact formation for Schottky and p-i-n samples, respectively. A thin (~100 Å) Au film was deposited as Schottky contact on the $Al_{0.38}Ga_{0.62}N$ layer. The p+ ohmic contacts were formed by Ni–Au metallization on the p+ GaN layer, followed by the same annealing process used for n+ contacts. Then, the device mesas, ranging from 30 to 200 $\mu$m in diameter were defined and isolated via RIE process. Afterwards, a ~100-nm-thick $Si_3N_4$ layer was deposited using plasma-enhanced chemical vapor deposition to passivate the sample surface and protect the thin Schottky contact films. In the final step, interconnect pads were formed by a ~0.7-$\mu$m-thick Ti–Au metallization. Fig. 1 shows the schematic of a completed Schottky photodiode.

The fabrication process of MSM photodiode samples started with the metallization of interdigitated back-to-back Schottky metal fingers. This was followed by mesa etch, surface passivation, and finally interconnect metallization. MSM photodiodes with equal finger spacings and widths varying between 3 and 10 $\mu$m were fabricated. The device mesas had an active area of $100 \times 100$ $\mu m^2$. Several microphotographs of completed samples are shown in Fig. 2.

### C. Characterization

After device fabrication, current–voltage ($I$–$V$), spectral responsivity, and high-speed characterizations were carried out. All measurements were made on-wafer, using a microwave probe station. To observe the electrical diode characteristics and the leakage current of the solar-blind AlGaN photodiodes, we

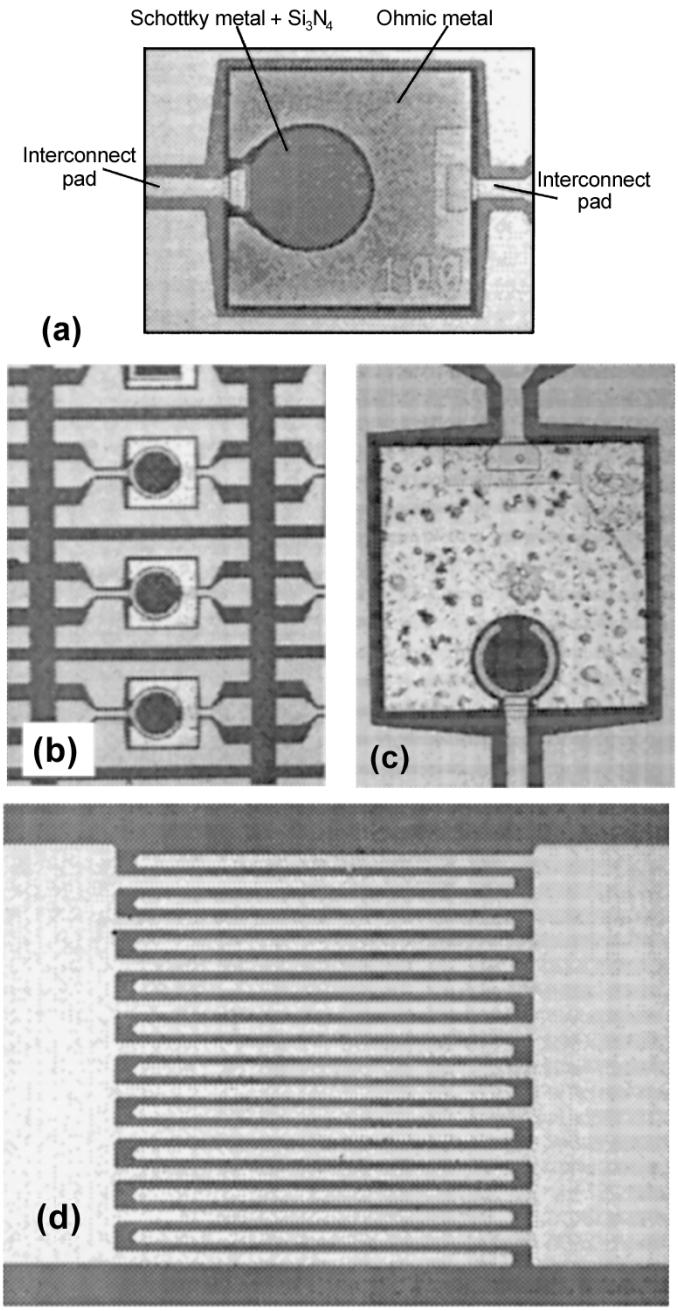


Fig. 2. Microphotographs of completed solar-blind devices. (a) Schottky photodiode with 100-$\mu$m diameter. (b) Several p-i-n photodiodes. (c) Small area (60 $\mu$m diameter) p-i-n photodiode. (d) MSM photodiode 3-$\mu$m fingers.

first performed the $I$–$V$ measurements. The measurement setup consisted of a high-resistance Keithley 6517A electrometer, dc probes with triax output and low-noise triax cables. The dc current was measured as voltage was applied to the devices.

Spectral responsivity measurements were done using a 175-W xenon light source, 1/4-m Digikrom DK240 monochromator, multimode UV fiber, dc voltage source, SR830 DSP lock-in amplifier, and a Newport model 1830-C calibrated optical power meter. Xenon lamp output was fed into the monochromator. The monochromator output was chopped and coupled to a multimode UV fiber using a UV-enhanced focusing lens. The detectors were illuminated by the optical

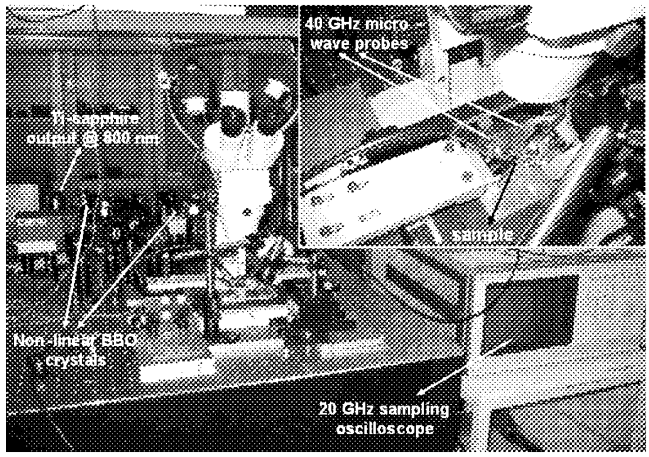


Fig. 3. High-frequency characterization setup for pulse-response measurements at 267 nm.

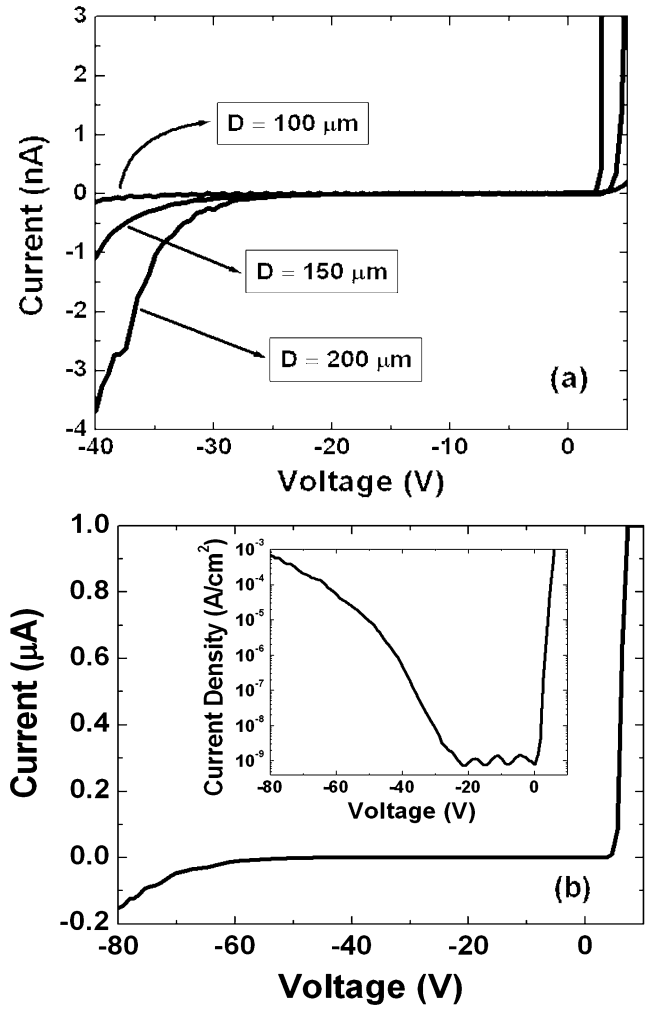


Fig. 4. (a) $I$–$V$ curves obtained from Schottky photodiodes with different device areas. (b) Dark current measurement of a $150 \times 150$ $\mu$m$^2$ device. Inset shows the corresponding dark current density.

output coming out from the fiber which was calibrated using the calibrated photodetector. The detectors were biased with a dc voltage source up to 50 V, and the resulting photocurrent was measured using the lock-in amplifier.

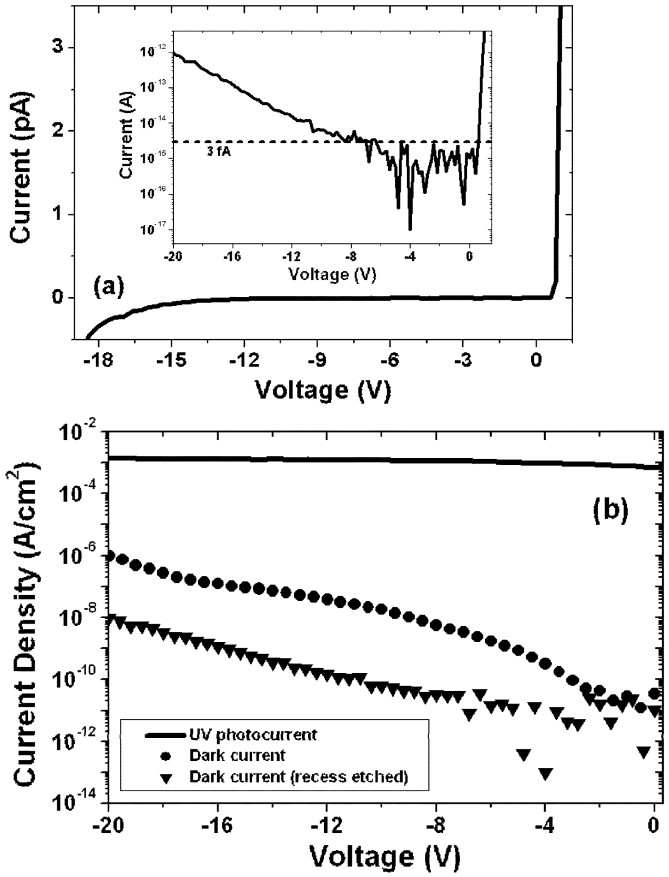


Fig. 5. (a) Dark current of a $100 \times 100$ $\mu m^2$ solar-blind AlGaN photodiode. Inset shows the same plot in logarithmic scale. (b) Dark current density before/after recess etch and UV photocurrent under 267-nm illumination.

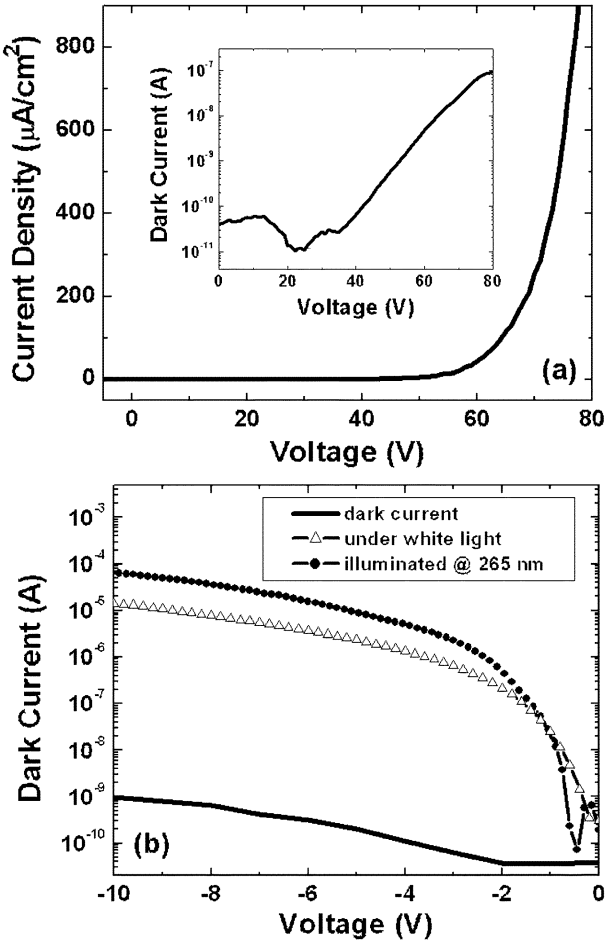


Fig. 6. (a) Dark current density of a solar-blind AlGaN MSM photodiode with 10-$\mu$m finger spacing. Inset shows the leakage current in logarithmic scale. (b) $I$–$V$ curves of a device with 5-$\mu$m finger spacing under different illumination conditions.

Temporal high-frequency measurements were done at the solar-blind wavelength of 267 nm. Ultrafast UV pulses were generated using a laser setup with two nonlinear crystals. A Coherent Mira 900F model femtosecond mode-locked Ti:sapphire laser was used to generate the pump beam at 800 nm. The pump pulses were produced with 76-MHz repetition rate and 140-fs pulse duration. These pulses were frequency doubled to generate a second harmonic beam at 400 nm using a 0.5-mm-thick type-I $\beta$-$BaB_2O_4$ (BBO) crystal. The second harmonic beam and the remaining part of the pump beam were frequency summed to generate a third harmonic output beam at 267 nm using another type-I BBO crystal with thickness of 0.3 mm. The resulting 267-nm pulses had pulsewidths below 1 ps and were focused on to the devices using UV-enhanced mirrors and lenses. The detectors were biased using a dc voltage source and a 26-GHz bias tee. Using a 40-GHz microwave probe and cables, the electrical pulses were transferred to a 20-GHz sampling oscilloscope where the temporal pulse responses were observed (Fig. 3).

## III. Results and Discussion

### A. Current–Voltage

All three detector samples exhibited excellent $I$–$V$ characteristics with low dark current and high breakdown voltages. The good $I$–$V$ results indicate the quality of growth and fabrication processes.

Fig. 4(a) shows the measured $I$–$V$ data taken from AlGaN Schottky photodiodes with different device areas. In general, better $I$–$V$ characteristics were observed for smaller devices. Typical breakdown voltages above 40 V and turn-on voltages around 2 V were measured for solar-blind Schottky photodiode samples. These devices exhibited subpicoampere dark currents at reverse bias values as high as 30 V. The dark current (density) measured from a $150 \times 150$ $\mu m^2$ device is shown in Fig. 4(b). The dark current was below 400 fA for reverse bias up to 25 V. This corresponds to a dark current density lower than 1.8 nA/cm$^2$.

AlGaN p-i-n photodiodes displayed even better $I$–$V$ characteristics, particularly in terms of dark current. With the removal of the top p+ GaN cap layer, dark current values went down to a few fA. Fig. 5(a) shows the measured dark current of a $100 \times 100$-$\mu m^2$ device after recess etch. For reverse bias values smaller than 6 V, the measured dark current fluctuated below the 3-fA level, which corresponds to a dark current density smaller than $3.0 \times 10^{-11}$ A/cm$^2$. Dark current was below 7 fA for reverse bias values up to 10 V. The measured forward turn-on voltages were small ($\sim$1 V) and reverse breakdown behavior was observed for reverse bias values over 40 V.

Fig. 5(b) shows the dark current density measured before and after recess etch and the UV photocurrent generated by the

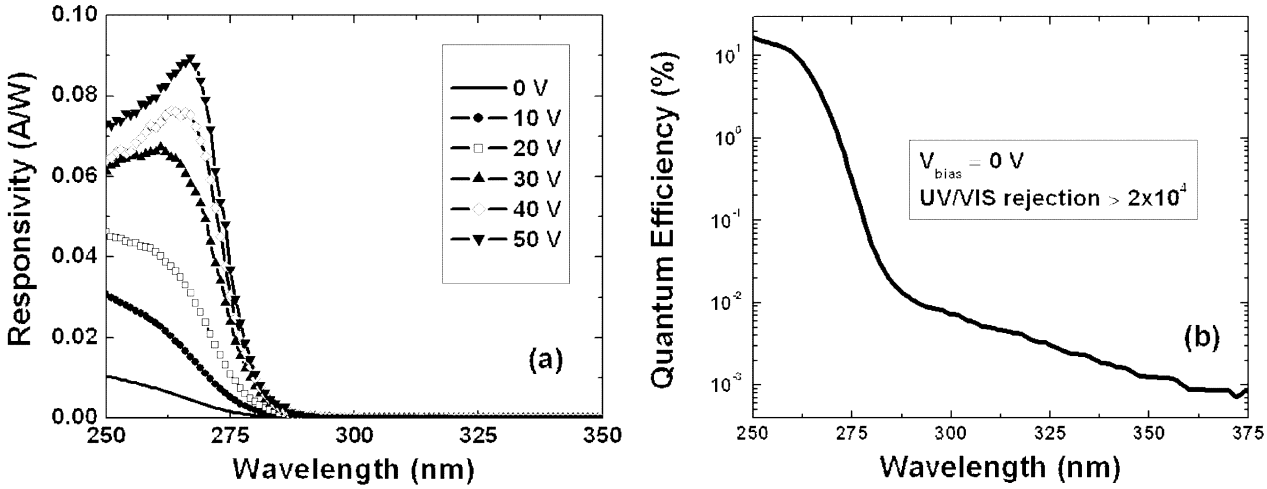


Fig. 7. (a) Measured spectral responsivity of the AlGaN Schottky photodiode as a function of reverse bias. (b) Zero bias spectral quantum efficiency of a solar-blind Schottky device.

photodiode under 267-nm illumination. The strong UV photocurrent shows that the detectors are operating in solar-blind spectrum. The dark current of the recess etched sample around zero bias is ∼8 orders of magnitude lower than the UV photocurrent. $I$–$V$ measurements showed that the dark current dropped by over two orders of magnitude after the GaN cap layer was removed. This result was well expected since the lower bandgap GaN layer generates more carriers due to thermal generation. Nevertheless, the dark current of the sample without recess etching was below 10 fA at 3-V reverse bias.

$I$–$V$ measurement of the AlGaN MSM sample resulted in higher leakage currents with respect to Schottky and p-i-n samples. The dark current measurement of a device with 10-$\mu$m finger spacing is shown in Fig. 6(a). The MSM photodiode exhibited a dark current density less than 1 $\mu$A/cm$^2$ at 40 V bias, along with a breakdown voltage in excess of 80 V. Subnanoampere dark current was observed at bias voltages as high as 54 V. Fig. 6(b) shows the $I$–$V$ characteristics of an MSM device with 5-$\mu$m finger spacing in dark, under UV (265 nm) and white-light illumination. This plot indicates the existence of UV photocurrent as a function of applied bias voltage.

### *B. Spectral Responsivity*

Spectral photoresponse measurements of the AlGaN photodiodes were carried out in the 250–400-nm spectral range. Bias-dependent spectral responsivity with true solar-blind characteristics was observed in all detector samples. All samples have exhibited true solar-blind operation. However, the cutoff characteristic of the p-i-n sample was not as good as Schottky and MSM devices.

Fig. 7(a) shows the measured spectral responsivity of a solar-blind Schottky photodiode under different bias conditions. The peak responsivity increased with applied reverse bias. It reached a maximum responsivity of 89 mA/W at 267 nm under 50-V reverse bias. The corresponding maximum quantum efficiency was calculated as 42%. The cutoff wavelength red shifted (from 266 to 274 nm) with increasing reverse bias. Since $\lambda_c < 280$ nm was satisfied, true solar-blind detection was successfully demonstrated. The zero-bias (photovoltaic) spectral quantum efficiency curve of another AlGaN Schottky device is shown in Fig. 7(b). The quantum efficiency drops sharply around 270 nm and a contrast of three orders of magnitude was already obtained around 280 nm. For $\lambda > 280$ nm, the responsivity decay continued with a lower rate and a maximum visible rejection of $2.4\times10^4$ was achieved at 350 nm. When reverse bias was applied, the rejection became weaker.

The spectral responsivity measurements of the AlGaN p-i-n sample were completed in several steps, as the absorbing GaN cap layer was etched step by step. The measurement results obtained before the recess-etch process are shown in Fig. 8(a). The device efficiency increased with applied reverse bias. Zero-bias peak efficiency of 22% at 267 nm improved to 43% at 271 nm for 20-V reverse bias. Quantum efficiency did not increase for higher reverse bias values, which indicates that the undoped $Al_{0.45}Ga_{0.55}N$ active layer was totally depleted at 20 V. The corresponding peak responsivity under full depletion was 95 mA/W at 271 nm. The cutoff wavelength of the p-i-n devices was around 283 nm. A visible rejection of ∼4 orders of magnitude was achieved at zero bias (see inset figure). The cutoff was rather smooth; three orders of magnitude rejection was reached within 100 nm.

To observe the effect of p+ GaN cap layer removal, this layer was recess etched in several steps. The corresponding responsivity curves at 10-V reverse bias for each etch step are shown in Fig. 8(b). As the p+ GaN cap layer was recess etched, less absorption loss within this layer resulted in higher device responsivity. The p+ GaN layer was completely etched in three etch steps. The peak responsivity improved from 81 to 111 mA/W, while the peak wavelength changed from 271 to 261 nm. The peak quantum efficiency performance achieved after three etch steps was 53% at 261 nm.

Fig. 9 shows the measured spectral responsivity curves of MSM devices under different bias conditions. The solar-blind MSM photodiodes have shown true solar-blind photoresponse with a cutoff wavelength of 272 nm. Photoconductive gain mechanism dominated the photoresponse for relatively low bias voltages. The peak responsivity under 6-V bias was measured as 1.26 A/W at 264 nm, corresponding to a peak quantum efficiency of ∼600%. The photoconductive gain in AlGaN MSM photodiodes can be explained by the presence

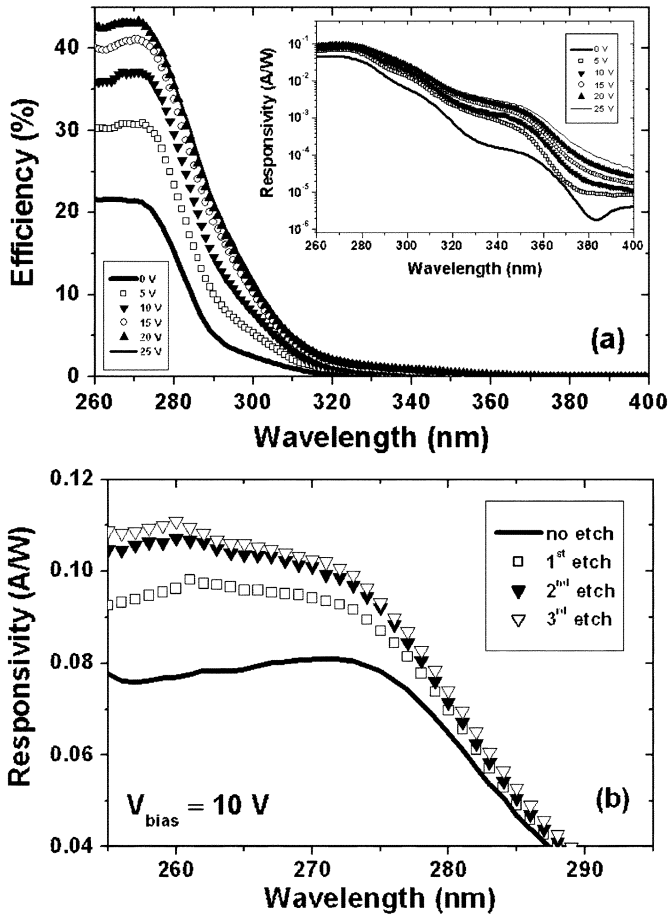


Fig. 8. (a) Spectral quantum efficiency and the corresponding responsivity curve of the nonetched solar-blind AlGaN p-i-n detector. (b) Spectral responsivity as a function of recess etch of the p+ GaN cap layer.

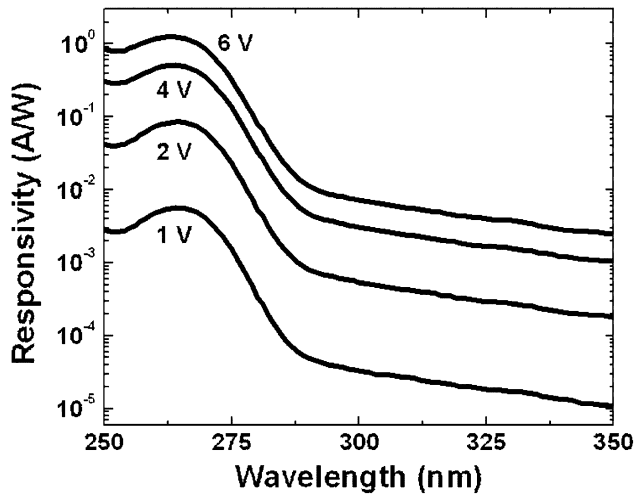


Fig. 9. Bias-dependent spectral responsivity curves of the solar-blind AlGaN MSM detector.

of hole-trapping sites due to threading dislocations [48]. Holes are accumulated at the trap sites, increasing the electron injection at the cathode. This injection results in photoconductive gain which is proportional to the electric field between the electrodes.

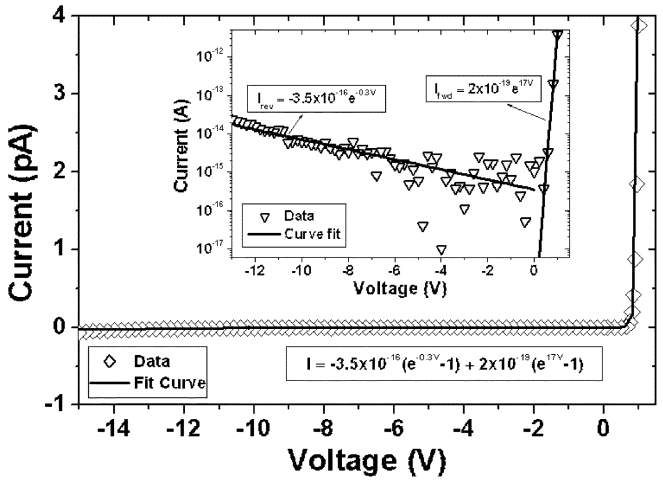


Fig. 10. Exponential curve fitting to the measured dark current of a $100 \times 100$ $\mu m^2$ AlGaN p-i-n detector. Inset figure shows the reverse and forward bias part fitting curves separately in a semi-log plot.

A sharp drop in responsivity around 275 nm was observed. A visible rejection of nearly three orders of magnitude was obtained at 350 nm. The rejection at longer wavelengths was measured using continuous wave Ar laser lines. Under zero bias, at 458 nm (the shortest line of Ar), the rejection was measured as $2\times10^4$.

### C. Detectivity

Based on the fact that the background radiation is very small with respect to the thermal noise within the solar-blind spectrum, we can safely assume that the detectivity of solar-blind detectors is thermally limited. Therefore, neglecting the background radiation component, the thermally limited specific detectivity can be calculated by $D^* = R_\lambda\ (R_0A/4\ \mathrm{kT})^{1/2}$, where $R_\lambda$ is the photovoltaic device reponsivity, $R_0$ is the dark impedance at zero bias which is also known as differential resistance, and $A$ is the detector area [49]. To calculate the thermally limited specific detectivity of our samples, $R_0$ was determined by fitting the dark current data with curve fitting method [50].

Fig. 10 shows the dark current measurement data of a $100 \times 100$ $\mu m^2$ AlGaN p-i-n device and the exponential fitting curve in both logarithmic and linear scale. By taking the derivative $(dV/dI)$ of the resulting curve equation at zero bias, we obtained a differential resistance of $R_0 = 9.52 \times 10^{15}\ \Omega$. Combining with $R_\lambda = 65$ mA/W, $A = 10^{-4}$ cm$^2$, and $T = 293$ K, we achieved a solar-blind detectivity performance of $D^* = 4.9 \times 10^{14}$ cmHz$^{1/2}$W$^{-1}$ at 267 nm for the AlGaN p-i-n sample. This value is even higher than the detectivity performance of a conventional PMT-based detector operating around 300 nm ($D^* \approx 4.0 \times 10^{14}$ cmHz$^{1/2}$W$^{-1}$) [51]. A similar procedure was applied to Schottky and MSM samples. As expected, lower detectivities were obtained for these samples mainly due to the higher leakage current and lower photovoltaic responsivity. Detectivity values of $5.6\times10^{12}$ cmHz$^{1/2}$W$^{-1}$ at 250 nm, and $8.9\times10^{10}$ cmHz$^{1/2}$W$^{-1}$ at 264 nm were achieved with AlGaN Schottky and MSM photodiodes. Table III summarizes the results of detectivity analysis.

TABLE III
DETECTIVITY ANALYSIS FOR SOLAR-BLIND ALGAN PHOTODIODES.

| Detector Type | $R_\lambda$ (A/W) | $R_0$ ($\Omega$) | $D^*$ ($cmHz^{1/2}W^{-1}$) |
|---|---|---|---|
| Schottky | 0.010 | $2.31 \nearrow 10^{13}$ | $5.6\times10^{12}$ |
| p-i-n | 0.065 | $9.52 \nearrow 10^{15}$ | $4.9\times10^{14}$ |
| MSM | 0.002 | $3.34 \nearrow 10^{11}$ | $8.9\times10^{10}$ |

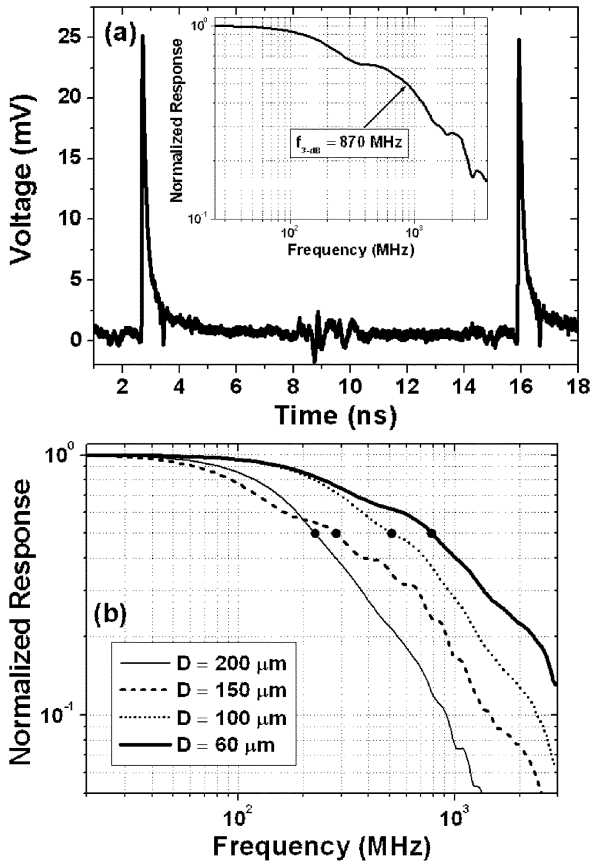


Fig. 11. (a) Pulse response of an 80-$\mu$m-diameter Schottky photodiode. Inset shows the FFT of temporal data. (b) Frequency response curves of Schottky detectors with different device areas. 3-dB bandwidths of 220, 280, 510, and 780 MHz were obtained with decreasing device area.

### D. Speed

Time-domain high-speed characterization of the solar-blind detector samples resulted in fast pulse responses with high 3-dB bandwidths. The detector pulse responses were bias dependent. The fastest pulses were produced by small-area devices. Very short rise times were observed. The response speed of the devices was limited by the slow decay tails.

For Schottky photodiodes, faster pulses were obtained for higher reverse bias values as the thick n-AlGaN absorption layer was fully depleted under high reverse bias voltages. The fastest pulse response was measured with an 80-$\mu$m-diameter device [Fig. 11(a)]. Under 15-V reverse bias, it produced a pulse response with a very fast rise time of 12 ps and a full-width at half-maximum (FWHM) of 216 ps. Using the fast Fourier transform (FFT), the corresponding 3-dB bandwidth was calculated as 870 MHz. Pulse responses with narrower pulsewidths were also measured, but their calculated 3-dB bandwidth was lower due to longer decay parts. Fig. 11(b) shows the device area dependence of the frequency response. The 3-dB bandwidths of 220, 280, 510, and 780 MHz were obtained with device diameters of 200, 150, 100, and 60 $\mu$m, respectively.

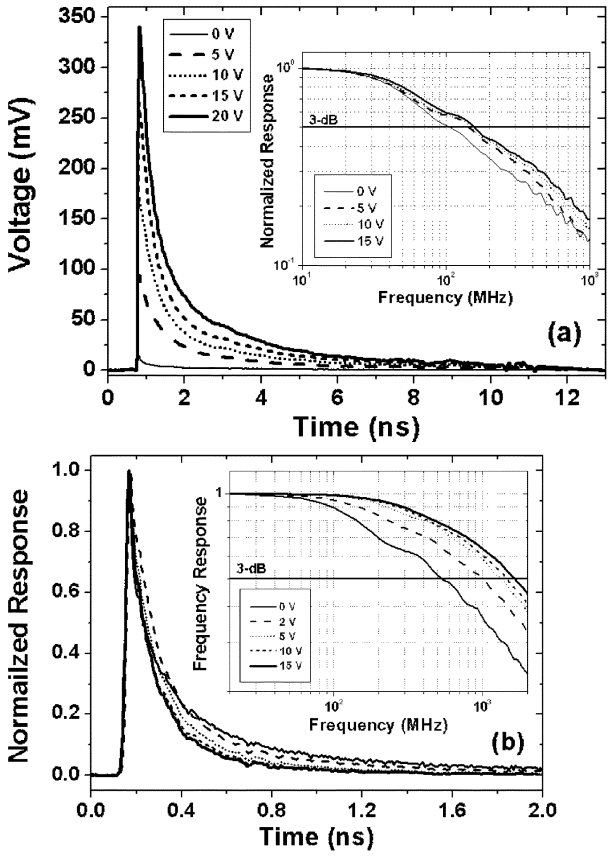


Fig. 12. (a) Pulse response of a 30-$\mu$m-diameter p-i-n photodiode before recess etch. Inset shows the FFT of temporal data. (b) Normalized pulse response of the same device after recess etch. Corresponding frequency response is shown in the inset figure.

To understand the relaxation mechanism of these devices, exponential fittings have been made to the measured pulse response. A good fit was realized with a second-order exponential decay with two different time constants, 103 ps and 2.63 ns. Both values are much larger than the carrier transit times and RC time constant of the device ($\sim$27 ps). This indicates that mechanisms other than RC and transit time limitations are responsible for the decay part of the high-speed response of these solar-blind detectors. We postulate that the long and multiexponential decay times are mainly related to trap centers in AlGaN. While moving toward the contact regions, photogenerated carriers can be trapped at these sites. The long decay tail is possibly formed by the arrival of such released carriers which are trapped in these sites for a rather long time. Another slowing mechanism may be the carrier diffusion component originating from low field regions close to the center of the mesa [34].

High-speed measurements for the p-i-n sample were done before and after recess etch. Fig. 12(a) and (b) shows the measured pulse response data of a 30-$\mu$m-diameter device with and without the p+ GaN cap layer, respectively. The calculated

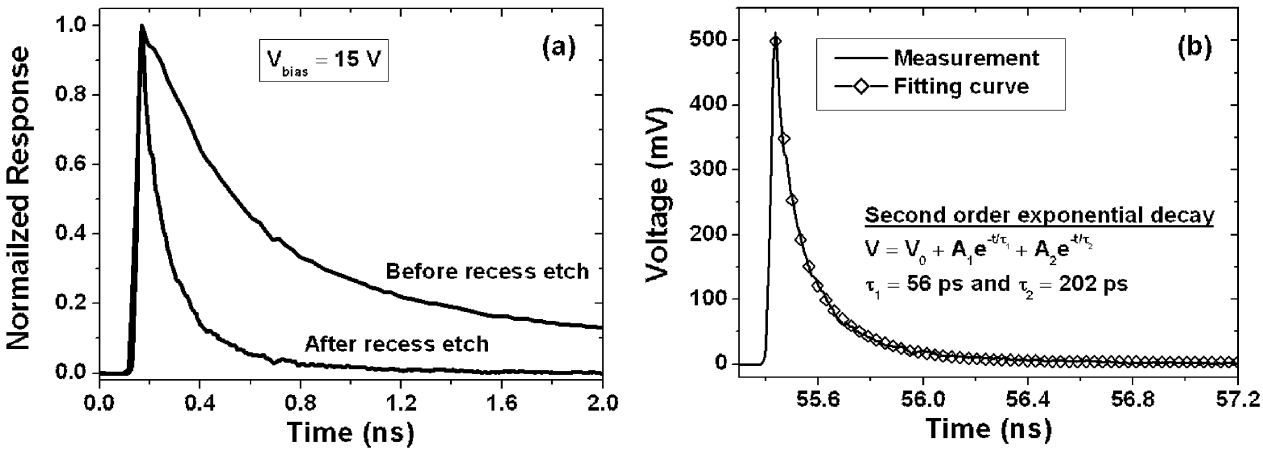


Fig. 13. (a) Normalized pulse response measurements of the AlGaN p-i-n photodiode before and after recess etch. (b) Curve fitting to the pulse response of the recess etched device.

FFT curves are also plotted. Parallel to theoretical expectations, faster response and higher 3-dB bandwidths were obtained after the removal of GaN cap layer. The p+ GaN layer is a low-field region, in which carriers move by diffusion. The minority carrier (electrons) diffusion mechanism limits the bandwidth of the nonetched p-i-n detector. After the removal of the GaN cap layer, the decay tail was reduced significantly: fall time decreased from 2.49 ns to 290 ps under 15-V reverse bias. At the same time, FWHM was improved from 384 to 71 ps. The detectors responded faster under higher reverse biases. FWHM values of 115 and 71 ps were measured for reverse bias values of 2 and 15 V, respectively. The fastest results were obtained at 15-V reverse bias. The 3-dB bandwidths achieved at 15 V bias were 160 MHz and 1.65 GHz for as-grown and recess-etched samples.

To make a better comparison, 15-V pulse responses are plotted in Fig. 13(a). Also, an exponential decay fit was applied to the recess etched device response. A good fit was accomplished using a second-order exponential decay with time constants of 56 and 202 ps [see Fig. 13(b)].

The measured pulse responses of AlGaN MSM photodiodes had short rise times and exponentially decaying fall times. Faster pulses were obtained with smaller finger spacings due to reduced carrier transit times. Therefore, the best high-speed results were achieved with 3-$\mu$m devices. Pulse response measurements under different bias conditions for the 3-$\mu$m device are plotted in Fig. 14(a). As expected, the pulse amplitudes had increased with applied bias voltage, due to larger photoconductive gain. Pulsewidths also increased with bias: 76-, 99-, 121-, and 133-ps FWHM values were measured at 5-, 10-, 15-, and 17-V bias, respectively. Hence, slower responses were obtained under larger bias and gain values. This result was confirmed with the FFT analysis of the temporal data. Fig. 14(b) shows the corresponding FFT curves of the measured pulse responses. A maximum 3-dB bandwidth of 5.4 GHz was achieved at 5-V bias. Bandwidth decreased with increasing bias: 3-dB bandwidths of 2.1, 1.7, and 1.5 GHz were obtained at 10-, 15-, and 17-V bias, respectively.

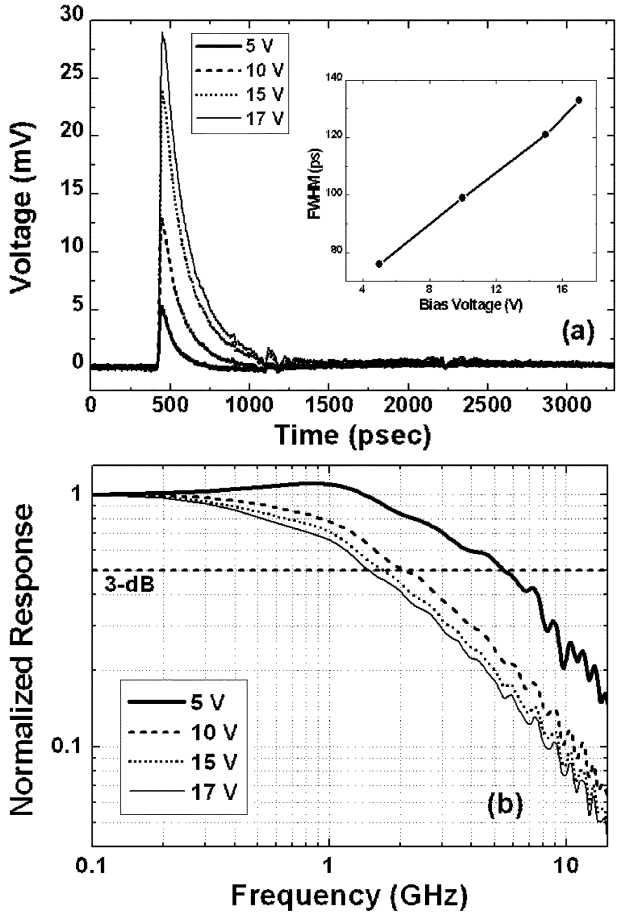


Fig. 14. (a) Bias-dependent temporal pulse responses of an AlGaN MSM photodiode with 3-$\mu$m finger spacing. Inset shows the measured FWHM values with respect to bias voltage. (b) Corresponding FFT curves.

## IV. Conclusion

We have designed, fabricated, and characterized high-performance AlGaN-based solar-blind heterojunction Schottky, p-i-n, and MSM photodiodes. True solar-blind operation was successfully demonstrated with all samples. The dark current, solar-blind detectivity, and high-speed results demonstrated in

this paper correspond to the best performances reported for AlGaN-based solar-blind photodetectors.

## REFERENCES


[1] P. Schreiber, T. Dang, G. Smith, T. Pickenpaugh, P. Gehred, and C. Litton, "Solar blind UV region and UV detector development objectives," *Proc. SPIE*, vol. 3629, pp. 230–248, 1999.

[2] M. Razeghi and A. Rogalski, "Semiconductor ultraviolet detectors," *J. Appl. Phys.*, vol. 79, pp. 7433–7473, 1996.

[3] E. Monroy, "III-nitride-based UV photodetectors," in *III-V Nitride Semiconductors Applications and Devices*, 1st ed, M. O. Manasreh, Ed. New York: Taylor and Francis, 2003, vol. 16, pp. 525–591.

[4] S. Strite and H. Morkoç, "GaN, AlN, and InN: A review," *J. Vac. Sci. Technol. A*, vol. 10, pp. 1237–1266, 1992.

[5] H. Morkoç, S. Strite, G. B. Gao, M. E. Lin, B. Sverdlov, and M. Burns, "Large-band-gap SiC, III-V nitride, and II-VI ZnSe-based semiconductor device technologies," *J. Appl. Phys.*, vol. 76, pp. 1363–1398, 1994.

[6] H. Morkoc *et al.*, "GaN based III-V nitrides by molecular beam epitaxy," *J. Cryst. Growth*, vol. 150, pp. 887–891, 1995.

[7] S. Sinharoy, G. Augustine, L. B. Rowland, A. K. Agarwal, R. L. Messham, M. C. Driver, and R. H. Hopkins, "Molecular beam epitaxy growth and characterization of GaN and $Al_xGa_{1-x}N$ on 6 H-SiC," *J. Vac. Sci. Technol. A*, vol. 14, pp. 896–899, 1996.

[8] D. Brunner, H. Angerer, E. Bustarret, F. Freudenberg, R. Höpler, R. Dimitrov, O. Ambacher, and M. Stutzmann, "Optical constants of epitaxial AlGaN films and their temperature dependence," *J. Appl. Phys.*, vol. 82, pp. 5090–5096, 1997.

[9] F. Omnès, N. Marenco, B. Beaumont, Ph. de Mierry, E. Monroy, F. Calle, and E. Muñoz, "Metalorganic vapor-phase epitaxy-grown AlGaN materials for visible-blind ultraviolet photodetector applications," *J. Appl. Phys.*, vol. 86, pp. 5286–5292, 1999.

[10] S. C. Jain, M. Willander, J. Narayan, and R. Van Overstraeten, "III-nitrides: Growth, characterization, and properties," *J. Appl. Phys.*, vol. 87, pp. 965–1006, 2000.

[11] H. K. Kwon, C. J. Eiting, D. J. H. Lambert, B. S. Shelton, M. M. Wong, T. G. Zhu, and R. D. Dupuis, "Optical properties of undoped and modulation-doped AlGaN/GaN single heterostructures grown by metalorganic chemical vapor deposition," *J. Appl. Phys.*, vol. 90, pp. 1817–1822, 2001.

[12] J. P. Zhang, H. M. Wang, M. E. Gaevski, C. Q. Chen, Q. Fareed, J. W. Yang, G. Simin, and M. A. Khan, "Crack-free thick AlGaN grown on sapphire using AlN/AlGaN superlattices for strain management," *Appl. Phys. Lett.*, vol. 80, pp. 3542–3544, 2002.

[13] C. Q. Chen, J. P. Zhang, M. E. Gaevski, H. M. Wang, W. H. Sun, R. S. Q. Fareed, J. W. Yang, and M. A. Khan, "AlGaN layers grown on GaN using strain-relief interlayers," *Appl. Phys. Lett.*, vol. 81, pp. 4961–4963, 2002.

[14] T. Akasaka, T. Nishida, Y. Taniyasu, M. Kasu, T. Makimoto, and N. Kobayashi, "Reduction of threading dislocations in crack-free AlGaN by using multiple thin $Si_xAl_{1-x}N$ interlayers," *Appl. Phys. Lett.*, vol. 83, pp. 4140–4142, 2003.

[15] J. C. Carrano, T. Li, P. A. Grudowski, R. D. Dupuis, and J. C. Campbell, "Improved detection of the invisible," *IEEE Circuits Devices Mag.*, vol. 15, pp. 15–24, 1999.

[16] D. Walker, X. Zhang, P. Kung, A. Saxler, S. Javapor, J. Xu, and M. Razeghi, "AlGaN ultraviolet photoconductors grown on sapphire," *Appl. Phys. Lett.*, vol. 68, pp. 2100–2101, 1996.

[17] B. W. Lim, Q. C. Chen, J. Y. Yang, and M. A. Khan, "High responsivity intrinsic photoconductors based on $Al_xGa_{1-x}N$," *Appl. Phys. Lett.*, vol. 68, pp. 3761–3762, 1996.

[18] A. Osinsky, S. Gangopadhyay, B. W. Lim, M. Z. Anwar, M. A. Khan, D. V. Kuksenkov, and H. Temkin, "Schottky barrier photodetectors based on AlGaN," *Appl. Phys. Lett.*, vol. 72, pp. 742–744, 1998.

[19] E. Monroy, F. Calle, J. L. Pau, F. J. Sanchez, E. Munoz, F. Omnes, B. Beaumont, and P. Gibart, "Analysis and modeling of $Al_xGa_{1-x}N$-based Schottky barrier photodiodes," *J. Appl. Phys.*, vol. 88, pp. 2081–2091, 2000.

[20] S. L. Rumyantsev, N. Pala, M. S. Shur, R. Gaska, M. E. Levinshtein, V. Adivarahan, J. Yang, G. Simin, and M. A. Khan, "Low-frequency noise in $Al_{0.4}Ga_{0.6}$ N-based Schottky barrier photodiodes," *Appl. Phys. Lett.*, vol. 79, pp. 866–868, 2001.

[21] V. Adivarahan, G. Simin, G. Tamulaitis, R. Srinivasan, J. Yang, M. A. Khan, M. S. Shur, and R. Gaska, "Indium-silicon co-doping of high-aluminum-content AlGaN for solar blind photodetectors," *Appl. Phys. Lett.*, vol. 79, pp. 1903–1905, 2001.

[22] N. Biyikli, O. Aytur, I. Kimukin, T. Tut, and E. Ozbay, "Solar-blind AlGaN-based Schottky photodiodes with low noise and high detectivity," *Appl. Phys. Lett.*, vol. 81, pp. 3272–3274, 2002.

[23] N. Biyikli, I. Kimukin, T. Kartaloglu, O. Aytur, and E. Ozbay, "High-speed solar-blind photodetectors with indium-tin-oxide Schottky contacts," *Appl. Phys. Lett.*, vol. 82, pp. 2344–2346, 2003.

[24] G. Parish, S. Keller, P. Kozodoy, J. P. Ibbetson, H. Marchand, P. T. Fini, S. B. Fleischer, S. P. Denbaars, U. K. Mishra, and E. J. Tarsa, "High-performance (Al,Ga)N-based solar-blind ultraviolet p-i-n detectors on laterally epitaxially overgrown GaN," *Appl. Phys. Lett.*, vol. 75, pp. 247–249, 1999.

[25] D. Walker, V. Kumar, K. Mi, P. Sandvik, P. Kung, X. H. Zhang, and M. Razeghi, "Solar-blind AlGaN photodiodes with very low cutoff wavelength," *Appl. Phys. Lett.*, vol. 76, pp. 403–405, 2000.

[26] E. J. Tarsa, P. Kozodoy, J. Ibbetson, B. P. Keller, G. Parish, and U. Mishra, "Solar-blind AlGaN-based inverted heterostructure photodiodes," *Appl. Phys. Lett.*, vol. 77, pp. 316–318, 2000.

[27] D. J. H. Lambert, M. M. Wong, U. Chowdhury, C. Collins, T. Li, H. K. Kwon, B. S. Shelton, T. G. Zhu, J. C. Campbell, and R. D. Dupuis, "Back illuminated AlGaN solar-blind photodetectors," *Appl. Phys. Lett.*, vol. 77, pp. 1900–1902, 2000.

[28] J. D. Brown, J. Li, P. Srinivasan, J. Matthews, and J. F. Schetzina, "Solar-blind AlGaN heterostructure photodiodes," in *MRS Internet J. Nitride Semicond. Res.*, vol. 5, 2000, p. 9.

[29] M. M. Wong, U. Chowdhury, C. J. Collins, B. Yang, J. C. Denyszyn, K. S. Kim, J. C. Campbell, and R. D. Dupuis, "High quantum efficiency AlGaN/GaN solar-blind photodetectors grown by metalorganic chemical vapor deposition," *Phys. Stat. Sol. (A)*, vol. 188, pp. 333–336, 2001.

[30] P. Sandvik, K. Mi, F. Shahedipour, R. McClintock, A. Yasan, P. Kung, and M. Razeghi, "$Al_xGa_{1-x}N$ for solar-blind UV detectors," *J. Crystal Growth*, vol. 231, pp. 366–370, 2001.

[31] G. Parish, M. Hansen, B. Moran, S. Keller, S. P. Denbaars, and U. K. Mishra, "Solar-blind p-GaN/i-AlGaN/n-AlGaN ultraviolet photodiodes on SiC substrate," *Phys. Stat. Sol. (A)*, vol. 188, pp. 297–300, 2001.

[32] A. Hirano, C. Pernot, M. Iwaya, T. Detchprohm, H. Amano, and I. Akasaki, "Demonstration of flame detection in room light background by solar-blind AlGaN pin photodiode," *Phys. Stat. Sol. (A)*, vol. 188, pp. 293–296, 2001.

[33] J. C. Campbell, C. J. Collins, M. M. Wong, U. Chowdhury, A. L. Beck, and R. D. Dupuis, "High quantum efficiency at low bias $Al_xGa_{1-x}N$ p-i-n photodiodes," *Phys. Stat. Sol. (A)*, vol. 188, pp. 283–287, 2001.

[34] T. Li, D. J. H. Lambert, M. M. Wong, C. J. Collins, B. Yang, A. L. Beck, U. Chowdhury, R. D. Dupuis, and J. C. Campbell, "Low-noise back-illuminated $Al_xGa_{1-x}$ N-based p-i-n solar-blind ultraviolet photodetectors," *IEEE J. Quantum Electron.*, vol. 37, pp. 538–545, 2001.

[35] V. V. Kuryatkov, H. Temkin, J. C. Campbell, and R. D. Dupuis, "Low-noise photodetectors based on heterojunctions of AlGaN-GaN," *Appl. Phys. Lett.*, vol. 78, pp. 3340–3342, 2001.

[36] C. J. Collins, U. Chowdhury, M. M. Wong, B. Yang, A. L. Beck, R. D. Dupuis, and J. C. Campbell, "Improved solar-blind detectivity using an $Al_xGa_{1-x}N$ heterojunction p-i-n photodiode," *Appl. Phys. Lett.*, vol. 80, pp. 3754–3756, 2002.

[37] ——, "Improved solar-blind external quantum efficiency of back-illuminated $Al_xGa_{1-x}N$ heterojunction p-i-n photodiodes," *Electron. Lett.*, vol. 38, pp. 824–826, 2002.

[38] U. Chowdhury, M. M. Wong, C. J. Collins, B. Yang, J. C. Denyszyn, J. C. Campbell, and R. D. Dupuis, "High-performance solar-blind photodetector using an $Al_xGa_{1-x}N$ n-type window layer," *J. Cryst. Growth*, vol. 248, pp. 552–555, 2003.

[39] T. Li, D. J. H. Lambert, A. L. Beck, C. J. Collins, B. Yang, M. M. Wong, U. Chowdhury, R. D. Dupuis, and J. C. Campbell, "Solar-blind $Al_xGa_{1-x}$ N-based metal-semiconductor-metal photodetectors," *Electron. Lett.*, vol. 36, pp. 1581–1583, 2000.

[40] B. Yang, D. J. H. Lambert, T. Li, C. J. Collins, M. M. Wong, U. Chowdhury, R. D. Dupuis, and J. C. Campbell, "High-performance back-illuminated solar-blind AlGaN metal-semiconductor-metal photodetectors," *Electron. Lett.*, vol. 36, pp. 1866–1867, 2000.

[41] J. Y. Duboz, J. L. Reverchon, D. Adam, B. Damilano, F. Semond, N. Grandjean, and J. Massies, "High performance solar blind detectors based on AlGaN grown by MBE on Si," *Phys. Stat. Sol. (A)*, vol. 188, pp. 325–328, 2001.

[42] J. L. Pau, E. Monroy, E. Munoz, F. Calle, M. A. Sanchez-Garcia, and E. Calleja, "Fast AlGaN metal-semiconductor-metal photodetectors grown on Si(111)," *Electron. Lett.*, vol. 37, pp. 239–240, 2001.
[43] J. L. Pau, E. Munoz, M. A. Sanchez-Garcia, and E. Calleja, "Visible and solar-blind AlGaN metal-semiconductor-metal photodetectors grown on Si(111) substrates," *Phys. Stat. Sol. (A)*, vol. 192, pp. 314–319, 2002.
[44] J. Y. Duboz, J. L. Reverchon, D. Adam, B. Damilano, N. Grandjean, F. Semond, and J. Massies, "Submicron metal-semiconductor-metal ultraviolet detectors based on AlGaN grown on silicon: Results and simulation," *J. Appl. Phys.*, vol. 92, pp. 5602–5604, 2002.
[45] V. Kuryatkov, A. Chandolu, B. Borisov, G. Kipshidze, K. Zhu, S. Nikishin, H. Temkin, and M. Holtz, "Solar-blind ultraviolet photodetectors based on superlattices of AlN/AlGa(In)N," *Appl. Phys. Lett.*, vol. 82, pp. 1323–1325, 2003.
[46] E. Ozbay, I. Kimukin, N. Biyikli, O. Aytur, M. Gokkavas, G. Ulu, M. S. Unlu, R. P. Mirin, K. A. Bertness, and D. H. Christensen, "High-speed $>90\%$ quantum efficiency p-i-n photodiodes with a resonance wavelength adjustable in the 795–835 nm range," *Appl. Phys. Lett.*, vol. 74, pp. 1072–1074, 1999.
[47] N. Biyikli, T. Kartaloglu, O. Aytur, I. Kimukin, and E. Ozbay, "High-speed visible-blind GaN-based indium-tin-oxide Schottky photodiodes," *Appl. Phys. Lett.*, vol. 79, pp. 2838–2840, 2001.
[48] M. Ito, O. Wada, K. Nakai, and T. Sakurai, "Monolithic integration of a metal-semiconductor-metal photodiode and a GaAs preamplifier," *IEEE Electron. Dev. Lett.*, vol. 5, p. 531, 1984.
[49] S. Donati, *Photodetectors: Devices, Circuits, and Applications*. Upper Saddle River, NJ: Prentice-Hall, 2000.
[50] C. J. Collins, T. Li, D. J. H. Lambert, M. M. Wong, R. D. Dupuis, and J. C. Campbell, "Selective regrowth of $Al_{0.30}Ga_{0.70}N$ p-i-n photodiodes," *Appl. Phys. Lett.*, vol. 77, pp. 2810–2812, 2000.
[51] J. D. Brown, Z. Yu, J. Matthews, S. Harney, J. Boney, J. F. Schetzina, J. D. Benson, K. W. Dang, C. Terrill, T. Nohava, W. Yang, and S. Krishnankutty, "Visible-blind UV digital camera based on a $32 \times 32$ array of GaN/AlGaN p-i-n photodiodes," in *MRS Internet J. Nitride Semicond. Res.*, vol. 4, 1999, p. 9.

**Ekmel Ozbay** (M'98) was born on March 25, 1966, in Ankara, Turkey. He received the B.S. degree in electrical engineering from the Middle East Technical University, Ankara, in 1983 and the M.S. and Ph.D. degrees in electrical engineering from Stanford University, Stanford, CA, in 1989 and 1992.

From 1992 to 1994, he worked as a Scientist at the DOE Ames National Laboratory, Iowa State University, in the area of photonic bandgap materials. He joined the faculty of the Physics Department, Bilkent University, Ankara, in December 1994, where he is currently a Full Professor. His research includes GaN-based devices, photonic crystals, silicon micromachining, and high-speed optoelectronics. He has authored or coauthored more than 160 articles in scientific journals, conference proceedings, and books.

Dr. Ozbay is the 1997 recipient of the Adolph Lomb Medal of Optical Society of America. He is currently acting as a Topical Editor for *Optics Letters*.

**Necmi Biyikli** (S'01) was born in Utrecht, The Netherlands, in 1974. He received the B.S. and M.S. degrees in electrical and electronics engineering from Bilkent University, Ankara, Turkey, in 1996 and 1998, respectively. Currently he is working toward the Ph.D. degree at the same institution.

He has worked with AlGaAs, InAlGaAs/InP, InSb/InAs, and GaN/AlGaN material systems. During his Ph.D. research, he has (co)authored more than 30 refereed journal articles and conference proceedings. His research interests include design, fabrication, and characterization of high-performance photodetectors, high-speed optoelectronic devices, solar-blind UV photodiodes, III-nitride alloys, wide bandgap semiconductors, and physics and applications of nanostructures, nanoscale photonics, and electronic devices.

**Ibrahim Kimukin** (S'02) was born in Edirne, Turkey, in 1976. He received the B.S. degree in physics from Middle East Technical University, Ankara, Turkey in 1997. He received the M.S. degree from Bilkent University, Ankara, and is currently working toward the Ph.D. degree there.

In his research, he designed, fabricated and tested photodetectors grown with III–V semiconductor materials such as GaAs, AlAs, AlGaAs, InGaAs, InAlAs, InP, InGaAsP, InAs, InSb, and GaSb. He also worked on wide-bandgap materials such as GaN, and AlGaN for high-performance solar blind photodetectors. He has (co)authored more than 30 journal papers and conference proceedings.

**Tolga Kartaloğlu** (M'90) received the B.Sc. degree from the Department of Electrical and Electronics Engineering, Middle East Technical University, Ankara, Turkey, in 1994 and the M.Sc. and Ph.D. degrees from the Department of Electrical and Electronics Engineering, Bilkent University, Ankara, in 1996 and 2002, respectively.

Currently, he is with ASELSAN Inc., Ankara, as a Senior Engineer. His research interests include lasers, nonlinear optics, wavelength conversion, and optical parametric oscillators and amplifiers.

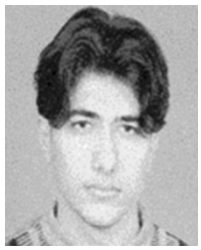

**Turgut Tut** was born on December 29, 1978, in Mersin, Turkey. He received the B.S. and M.S. degrees in physics from Bilkent University, Ankara, Turkey, in 2001 and 2004, respectively. Currently, he is pursuing the Ph.D. degree at the same university.

His research interests include design and fabrication of AlGaN–GaN-based solar-blind Schottky photodetectors.

**Orhan Aytür** (M'94–SM'00) was born in Ankara, Turkey, in 1965. He received the B.S. degree in electrical engineering from Middle East Technical University, Ankara, Turkey, in 1986, and the M.S. and Ph.D. degrees in electrical engineering from Northwestern University, Evanston, IL, in 1988 and 1991.

He worked as a Laser Scientist at Fibertek, Inc., and as a Research Associate at the University of New Mexico in 1991 and 1992. He joined the Department of Electrical Engineering, Bilkent University, Ankara, in 1993, where he is presently a Professor. His research interests include nonlinear frequency conversion of lasers, quantum optics, and high-performance photodetectors.